remote sensing

MDPI

Article

Estimation of Winter Wheat Stem Biomass by a Novel Two-Component and Two-Parameter Stratified Model Using Proximal Remote Sensing and Phenological Variables

Weinan Chen [1,2], Guijun Yang [1,2,*], Yang Meng [2,3], Haikuan Feng [2,3], Heli Li [2], Aohua Tang [1,2], Jing Zhang [1], Xingang Xu [2], Hao Yang [2], Changchun Li [4] and Zhenhong Li [1]

[1] College of Geological Engineering and Geomatics, Chang'an University, Xi'an 710054, China; 2022026021@chd.edu.cn (W.C.); 2022126042@chd.edu.cn (A.T.); 2020126044@chd.edu.cn (J.Z.); zhenhong.li@chd.edu.cn (Z.L.)

[2] Key Laboratory of Quantitative Remote Sensing in Agriculture of Ministry of Agriculture and Rural Affairs, Information Technology Research Center, Beijing Academy of Agriculture and Forestry Sciences, Beijing 100097, China; mengy@nercita.org.cn (Y.M.); fenghk@nercita.org.cn (H.F.); lihl@nercita.org.cn (H.L.); xuxg@nercita.org.cn (X.X.); yangh@nercita.org.cn (H.Y.)

[3] College of Agriculture, Nanjing Agricultural University, Nanjing 210095, China

[4] Institute of Quantitative Remote Sensing and Smart Agriculture, School of Surveying and Mapping Land Information Engineering, Henan Polytechnic University, Jiaozuo 454000, China; lcc@hpu.edu.cn

* Correspondence: yanggj@nercita.org.cn; Tel.: +86-10-5150-3647

Abstract: The timely and precise estimation of stem biomass is critical for monitoring the crop growing status. Optical remote sensing is limited by the penetration of sunlight into the canopy depth, and thus directly estimating winter wheat stem biomass via canopy spectra remains a difficult task. There is a stable linear relationship between the stem dry biomass (SDB) and leaf dry biomass (LDB) of winter wheat during the entire growth stage. Therefore, this study comprehensively considered remote sensing and crop phenology, as well as biomass allocation laws, to establish a novel two-component (LDB, SDB) and two-parameter (phenological variables, spectral vegetation indices) stratified model (Tc/Tp-SDB) to estimate SDB across the growth stages of winter wheat. The core of the Tc/Tp-SDB model employed phenological variables (e.g., effective accumulative temperature, EAT) to correct the SDB estimations determined from the LDB. In particular, LDB was estimated using spectral vegetation indices (e.g., red-edge chlorophyll index, $CI_{red\ edge}$). The results revealed that the coefficient values (β_0 and β_1) of ordinary least squares regression (OLSR) of SDB with LDB had a strong relationship with phenological variables. These coefficient (β_0 and β_1) relationships were used to correct the OLSR model parameters based on the calculated phenological variables. The EAT and $CI_{red\ edge}$ were determined as the optimal parameters for predicting SDB with the novel Tc/Tp-SDB model, with r, RMSE, MAE, and distance between indices of simulation and observation (DISO) values of 0.85, 1.28 t/ha, 0.95 t/ha, and 0.31, respectively. The estimation error of SDB showed an increasing trend from the jointing to flowering stages. Moreover, the proposed model showed good potential for estimating SDB from UAV hyperspectral imagery. This study demonstrates the ability of the Tc/Tp-SDB model to accurately estimate SDB across different growing seasons and growth stages of winter wheat.

Keywords: winter wheat; stem dry biomass; phenological scale; hyperspectral remote sensing; Tc/Tp-SDB stratified model

Citation: Chen, W.; Yang, G.; Meng, Y.; Feng, H.; Li, H.; Tang, A.; Zhang, J.; Xu, X.; Yang, H.; Li, C.; et al. Estimation of Winter Wheat Stem Biomass by a Novel Two-Component and Two-Parameter Stratified Model Using Proximal Remote Sensing and Phenological Variables. *Remote Sens.* **2024**, *16*, 4300. https://doi.org/10.3390/rs16224300

Academic Editor: Guido D'Urso

Received: 11 October 2024
Revised: 7 November 2024
Accepted: 16 November 2024
Published: 18 November 2024

1. Introduction

Winter wheat is the most important food crop in the world, and its planting and production are essential to ensure national food security and social stability [1–3]. Aboveground biomass (AGB) is an important indicator of crop yield and is often used to

diagnose the health of crops. AGB includes the biomass of crop leaves, stems, grains and other organs.

A key component of AGB is stem dry biomass (SDB), an important agronomic trait for the efficient transportation of water and nutrients. In general, healthy stems can be converted into good-quality silage, which can be used as fodder for livestock [4]. Stem biomass estimations can help farmers make more accurate decisions regarding whether to return crop residue to the field [5]. Moreover, stem biomass is also a key parameter in research on the global carbon cycle [6,7].

Stem biomass is traditionally estimated using destructive sampling, which is laborious, time-consuming, and cannot be easily extended to large areas [8,9]. Due to advantages such as non-destructive and rapid measurements, remote sensing technology has been widely used in biomass monitoring on scales ranging from individual fields to entire nations. Numerous advanced remote sensing sensors have been used to acquire vegetation canopy information, such as multispectral [10–12], hyperspectral [13–15], light detection and ranging (LiDAR) [16,17], and synthetic aperture radar (SAR) sensors [18,19]. Among these sensor technologies, hyperspectral sensors can obtain comprehensive spectral information from visible to near-infrared wavelengths [15,20]. This technology has shown great potential for dynamic crop growth monitoring.

However, due to the limited penetration capability of optical remote sensing techniques, the contribution of crop stems to the canopy spectrum is far less than that of leaves under vertical observation conditions in cases of high canopy coverage [21,22]. As a consequence, the canopy spectrum is mainly derived from the contribution of the canopy leaf [23]. In general, leaf dry biomass (LDB) is defined as the product of the leaf dry matter content and the leaf area index. Wang et al. explored the potential of the normalized dry matter index (NDMI) to estimate LDB in green canopies [24]. Moreover, Zhao et al. used the red-edge chlorophyll index ($CI_{red\ edge}$) to establish an empirical regression model to estimate the LDB of winter wheat based on vertical observations [25]. However, the canopy spectra used in the aforementioned studies were obtained under vertical observation conditions. Due to the low exposure of standing stems to the sensor, such methods of estimating LDB may not accurately estimate stem biomass.

According to the partitioning law of above-ground dry matter, there is a stable linear relationship between stem dry biomass and leaf dry biomass in a single growth stage. Therefore, when only limited canopy stem information is available through remote sensing, stem biomass may be accurately estimated based on leaf biomass. Yue et al. found that the slope coefficients of linear regression models between LDB and SDB tend to increase linearly as the growth stage progresses [26]. Similarly, Cheng et al. found comparable biomass partitioning patterns of stem and leaf in paddy rice [27]. Therefore, the change in the relationship between LDB and SDB with growth phase can be attributed to allometric-based regulation [28–30]. Given that the partition of crop organ biomass is related to the growth stage, it is obviously unrealistic to apply a single regression model to the entire growth period.

Phenology has direct and indirect effects on crop growth, development, and biomass allocation [31,32]. The Zadok scale was developed to describe cereal growth stages and is widely used in wheat research [33,34]. Han et al. integrated the Zadok scale into the RFR model to accurately estimate AGB for winter wheat [35]. However, the Zadok scale requires field observations as an input. Indicators related to thermal metrics or time, such as growing degree-days (GDD) and days after sowing (DAS), which are more readily available, are also used to indicate phenological growth stages [36]. Therefore, we hypothesized that phenological indicators could characterize the evolving relationship between stem biomass estimation models at different growth stages.

Based on the results obtained in the analysis described above, we proposed a novel method for the estimation of crop stem biomass using two components (LDB, SDB) and two parameters (VI, PV), designated as the Tc/Tp-SDB model. The main objectives of this study are to: (a) evaluate the performance of dry matter indices and chlorophyll indices

for the estimation of leaf biomass in winter wheat; (b) explore the dynamic mechanisms underlying the relationships between winter wheat dry biomass components and growth stages; (c) establish a two-component and two-parameter stratified model (Tc/Tp-SDB) for SDB estimations using proximal remote sensing and phenological variables.

2. Materials and Methods

2.1. Study Area and Experimental Design

Four winter wheat field experiments were conducted at the Xiao Tangshan National Precision Agriculture Research Center (116°26′36″E, 40°10′44″N) in Changping District, Beijing City, China (Figure 1a,b). The winter wheat in the study region is typically planted in late September or early October each year and harvested in mid-to-early June of the following year. The experiments included different nitrogen treatments, irrigation rates, and winter wheat cultivars across various years (Table 1).

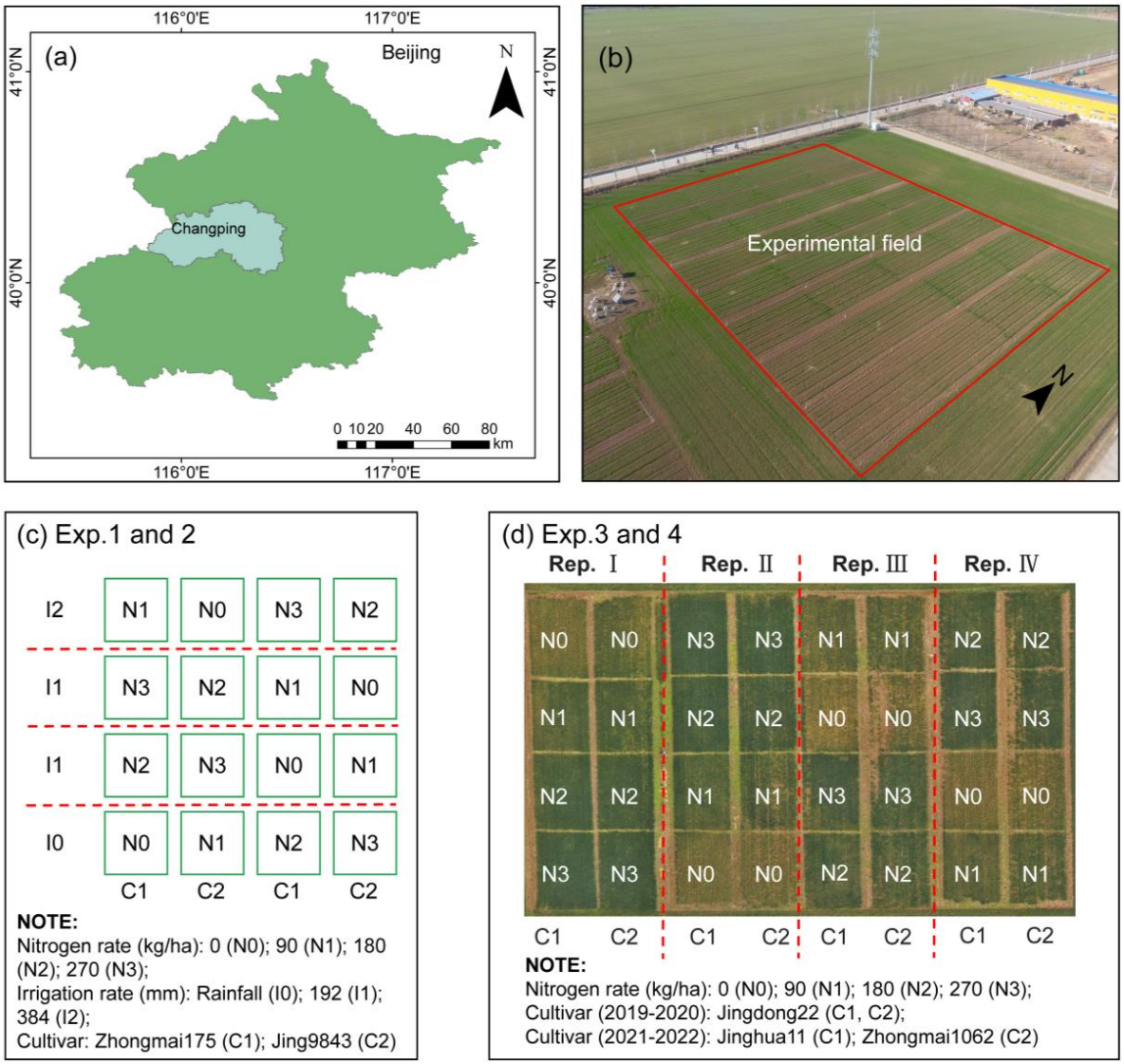

Figure 1. Geographical location of the study area and winter wheat field experiment. (**a**) Location of all experiments; (**b**) the layout of the experimental plots during 2019–2020; (**c**) experimental designs conducted during 2013–2015 (Exp. 1 and Exp. 2); (**d**) experimental designs conducted during 2019–2020 and 2021–2022 (Exp. 3 and Exp. 4).

Table 1. Summary of field treatments adopted for the experiment.

	Cultivar	Plots	Nitrogen Rate (kg/ha)	Irrigation Rate (mm)	Sampling Data
Exp. 1 (2013–2014)	Zhongmai175 Jing9843	16	N0 (0) N1 (90) N2 (180) N3 (270)	I0 (rainfall) I1 (192) I2 (384)	4.11; 4.21; 5.07; 5.20
Exp. 2 (2014–2015)	Zhongmai175 Jing9843	16	N0 (0) N1 (90) N2 (180) N3 (270)	I0 (rainfall) I1 (192) I2 (384)	4.14; 4.27; 5.12; 5.26
Exp. 3 (2019–2020)	Jingdong22	32	N0 (18) N1 (90) N2 (180) N3 (270)	Rainfall	4.17; 4.28; 5.15; 6.01
Exp. 4 (2021–2022)	Jinghua11 Zhongmai1062	32	N0 (18) N1 (90) N2 (180) N3 (270)	Rainfall	4.18; 4.29; 5.10; 5.30

Experiments 1 (Exp. 1) and 2 (Exp. 2) (Figure 1c) were conducted from 2013 to 2015, with a field size of 32 m × 32 m. Exp. 1 and 2 adopted a completely randomized experimental design with two winter wheat varieties, three irrigation rates, and four nitrogen fertilizer application rates, without repeated experiments. Experiments 3 (Exp. 3) and 4 (Exp. 4) (Figure 1d) were conducted in 32 randomly selected plots using four nitrogen rates and four repeated experiments for two cultivars, with only one variety used in 2019–2020. The field size of Exp. 3 and 4 was 100 m × 60 m. Data were collected over four years, mainly during the jointing stage (S1), flag-picking stage (S2), flowering stage (S3), and filling stage (S4) of winter wheat. Data from Exp. 1 and Exp. 4 were used to calibrate the model, while data from Exp. 2 and Exp. 3 were used for model validation. Note that data with potential quality issues were eliminated prior to the modeling process.

2.2. Data Acquisition

2.2.1. Field Canopy Hyperspectral Reflectance Measurements

The field canopy spectra of all four winter wheat experiments were measured using an ASD Fieldspec Handheld Spectrometer (Analytical Spectral Devices, Boulder, CO, USA), with a view angle and spectral range of 25° and 350–2500 nm, respectively. The spectral resolution of the spectrometer was 3 nm@700 nm and 10 nm@1400 nm/2100 nm. The collected canopy reflectance data were resampled to 1 nm resolution (2151 bands in total from 350 to 2500 nm). The canopy spectral reflectance was measured between 11:00 a.m. and 2:00 p.m. under cloud-free conditions. The instrument was calibrated using a white reference panel ($BaSO_4$) before each measurement to minimize the effect of natural light variations. The probe was held ~1 m above the winter wheat canopy during measurements and kept horizontal. A total of 20 canopy reflectance spectra were collected at the center of each plot, and the average spectrum was calculated for each plot to reduce the effect of environmental variation using ViewSpecPro version 5.0 (Analytical Spectral Devices, Boulder, CO, USA). It is worth noting that before calculating the average spectral reflectance, we need to eliminate the spectral curves of non-vegetation.

2.2.2. UAV Hyperspectral Image Acquisition

We obtained UAV hyperspectral images on 26 April and 13 May 2015. The images were collected using a UHD 185 Firefly Sensor (Cubert GmbH, Ulm, Germany) mounted on a DJI S1000 UAV with eight rotors (SZ DJI Technology Co., Ltd., Shenzhen, China). The sensor captured 125 spectral bands between 450–950 nm, with a spectral resolution of 8 nm and spectral resampling at 4 nm. Data were collected at a flight altitude of 50 m above the ground at a fixed speed of 5 m/s. Cubert Cube-Pilot version 1.4 (Cubert GmbH, Ulm, Germany), Agisoft PhotoScan Professional version 1.1.6 (Agisoft LLC, St. Petersburg, Russia), and ENVI version 5.3 (HARRIS geospatial, Wokingham, UK) were used for image stitching and geometric and radiometric correction. Further details of the data collection and processing flows can be found in Yue et al. [37]. In addition, we used the average

interpolation method to spectrally resample the UAV hyperspectral image so that its resolution is consistent with the field spectral resolution.

2.2.3. Field Experiment Data Acquisition

A total of 20 winter wheat plants were collected from the field through destructive sampling and transferred to the laboratory. Several agronomic traits (LDB, SDB) were determined sequentially after completing stem and leaf separation. All samples (20 tillers) were dried in an oven before determining leaf, stem, and spike biomass using electronic scales (±0.01 g). SDB and LDB were calculated individually according to the dry sample weight and plant density in the plot. Winter wheat dry biomass was calculated using Equation (1):

$$\mathrm{LDB} = \frac{\mathrm{DML} \times \mathrm{T}}{20 \times \mathrm{A}} \times 10^{-2} \quad (1)$$

$$\mathrm{SDB} = \frac{\mathrm{DMS} \times \mathrm{T}}{20 \times \mathrm{A}} \times 10^{-2} \quad (2)$$

where DWL (g) is the dry biomass of the winter wheat leaf sample, DWS (g) is the dry biomass of the winter wheat stem sample, T is the number of counted tillers in the sample area, A (m^2) is the sample area, and a conversion factor of 10^{-2} is used to convert g/m^2 to t/ha.

2.2.4. Meteorological Data Collection and Calculation of Thermal Metric-Related Phenological Variables

ERA5, the fifth-generation reanalysis data product of the European Center for Medium-Range Weather Forecasting (ECWF), was used to calculate phenological variables related to thermal metrics. The daily minimum and maximum air temperatures at a height of 2 m were collected via the Climate Data Store Toolbox (CDS Toolbox, https://cds.climate.copernicus.eu/, accessed on 25 May 2023). ERA5 employs Coordinated Universal Time (UTC), which was converted to China Standard Time (CST) to ensure consistency with the rest of the datasets in the study. The daily average temperature (Figure 2), the base indicator for calculating phenological variables related to thermal metrics, was calculated by averaging the maximum and minimum temperatures. The variations in daily minimum, maximum, and average temperatures were minimal across growing seasons. The phenological variables GDD and effective accumulative temperature (EAT) [38], were calculated as follows:

$$\mathrm{GDD} = \sum_{\mathrm{DOY}=1}^{\mathrm{DOY}} \frac{(\mathrm{T_{max}} + \mathrm{T_{min}})}{2} - \mathrm{T_{base}} \quad (3)$$

$$\mathrm{EAT} = \sum_{\mathrm{DAS}=1}^{\mathrm{DAS}} \frac{(\mathrm{T_{max}} + \mathrm{T_{min}})}{2} \quad (4)$$

where T_{max} and T_{min} are the daily maximum and minimum temperatures (°C), respectively; T_{base} is the base temperature for winter wheat, set at 0 °C; DOY is the day of the year; and DAS is days after sowing. Note that a DOY value of 1 corresponds to 1 January, while DAS = 0 denotes the sowing day.

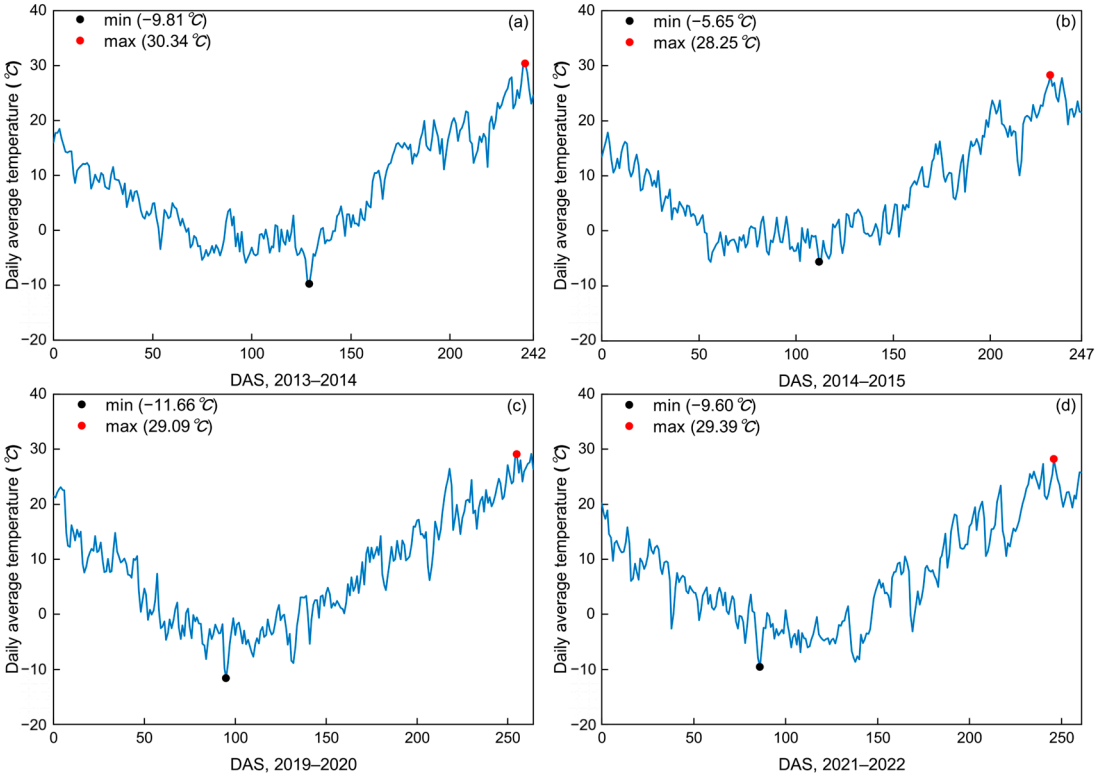

Figure 2. Daily average temperature during the four growing seasons of the study: (**a**) Exp. 1 (2013–2014); (**b**) Exp. 2 (2014–2015); (**c**) Exp. 3 (2019–2020); (**d**) Exp. 4 (2021–2022). Note: The sowing days (DAS = 0) of the four experiments were 1 October 2013, 7 October 2014, 27 September 2019, and 30 September 2021.

2.2.5. Spectral Vegetation Indices

Two groups of six vegetation indices (VIs) were calculated using the hyperspectral data (Table 2). One was the group of vegetation indices related to chlorophyll indices (CIs), including the Normalized Difference Vegetation Index (NDVI), the Red-edge Chlorophyll Index ($CI_{red\ edge}$), and the Simple Ratio 705 (SR_{705}). These CIs are widely used for estimating LAI and chlorophyll content. Moreover, they represent the red-edge-based index, ratio vegetation index, and the most commonly used normalized difference vegetation index. The other group consisted dry matter indices (DMIs), including the Normalized Difference index for the Leaf Mass per Area (ND_{LMA}), the Normalized Difference Lignin Index (NDLI), and the Normalized Difference Index for leaf canopy biomass (ND_{Bleaf}). The DMIs were less commonly used in the community due to the use of short-wavelength infrared (SWIR) bands. Moreover, the UHD 185 Firefly Sensor can not collect winter wheat canopy SWIR spectra. Thus, only the chlorophyll indices were used for winter wheat LDB estimation.

Table 2. Summary of spectral vegetation indices used in the study.

VI Type	VI	Formula	Reference
Chlorophyll indices	Normalized Difference Vegetation Index	$(R_{800} - R_{670})/(R_{800} + R_{670})$	[39]
	Red-edge Chlorophyll Index	$R_{800}/R_{720} - 1$	[40]
	Simple Ratio 705	R_{750}/R_{705}	[41]
Dry matter indices	Normalized Difference index for the Leaf Mass per Area	$(R_{1368} - R_{1722})/(R_{1368} + R_{1722})$	[42]
	Normalized Difference Lignin Index	$[\log(1/R_{1754}) - \log(1/R_{1680})]/[\log(1/R_{1754}) + \log(1/R_{1680})]$	[43]
	Normalized Difference Index for leaf canopy biomass	$(R_{1540} - R_{2160})/(R_{1540} + R_{2160})$	[44]

2.3. Cross-Validation for the Selection of the Optimal Vegetation Index

We attempted to select the optimal VI for LDB estimations from the two group of VIs in Table 2. This could help us select a vegetation index more suitable for LDB estimation. The distributions of the measured LDB and SDB from the calibration and validation datasets are shown in Figure 3. We observed differences in the distribution ranges of the two datasets, particularly for LDB, suggesting that the optimal VI selected using the calibration data could perform poorly when validating the datasets. To overcome this limitation, we used k-fold cross-validation to select the optimal VI [45], fully accounting for the calibration and validation datasets and addressing the problem posed by the limited number of samples. Here, we adopted 5-fold cross-validation for the model. First, all experimental data (n = 378) were randomly divided into five subsamples of the same size (m = 75). Next, four subsamples were cyclically utilized to calibrate the training model, while the remaining subsamples were employed as test data for performance evaluation. We then calculated the average test accuracy value to determine the optimal vegetation index for the VI-LDB method.

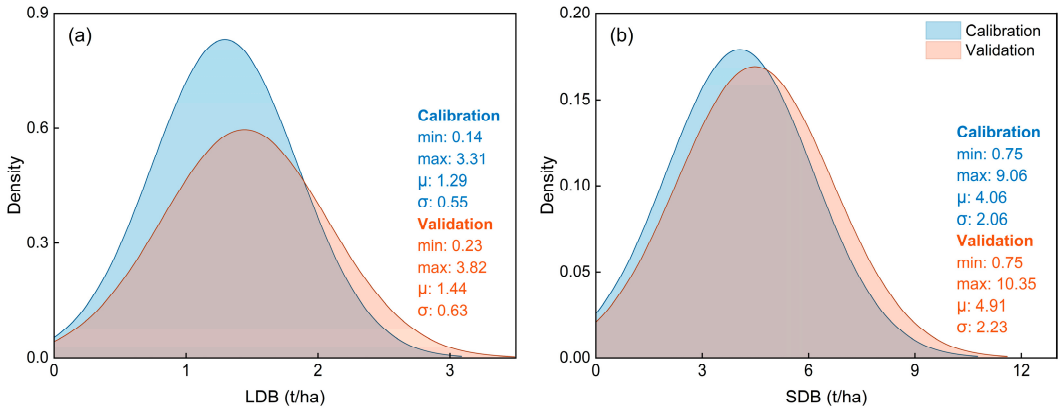

Figure 3. Distribution of the measured LDB (**a**) and SDB (**b**) for the calibration and validation datasets. The μ and σ represent average and standard deviation, respectively.

2.4. Estimation Model of Winter Wheat Stem Dry Biomass (Tc/Tp-SDB)

In this study, we proposed the Tc/Tp-SDB model, which spans different growth stages and employs phenological variables as constraints, to address two critical questions (Figure 4). The model was established using a stepwise procedure with two key steps.

In step 1, we explored the change law of different dry biomass components as growth stages progress to aid understanding of the dynamic changes in their relationships in the context of winter wheat phenology. It has been established that the effect of phenology is not necessarily required when estimating LDB [25]. Accordingly, the VI-LDB method was used to estimate LDB across growth stages. SDB was found to be greatly affected by phenology; thus, the effect of phenology must be considered when establishing an SDB estimation model.

For step 2, the theoretical structure of the Tc/Tp-SDB model was proposed as a two-level stratified model. A stratified model was introduced to calculate the phenological correction [25,46,47]. At level 1 (two-component level, Equation (5)), an ordinary least squares regression (OLSR) model of LDB and SDB was established for different growth periods. Due to the influence of phenology, the coefficients (β_0 and β_1) of the first level varied greatly with the growth stage. At level 2 (two-parameter level, Equations (6) and (7)), the phenological variable with the strongest correlations with the temporal (DOY and DAS) and thermal metrics (GDD and EAT) was used to correct the coefficients of the first level. In particular, LDB was estimated using the VI-LDB method, which was suitable for all growth stages. The regression form of VI-LDB can be linear, exponential or logarithmic.

$$\text{Level 1}: \ SDB = \beta_0 \times LDB + \beta_1 \tag{5}$$

$$\text{Level 2}: \ LDB = f(VI) \tag{6}$$

$$\beta_j = \gamma_{m0} \times PV + \gamma_{m1} \tag{7}$$

where β_0 and β_1 are the slope and intercept of the linear model at different growth stages at level 1, respectively; β_j corresponds to β_0 and β_1 from level 1; γ_{m0} and γ_{m1} are the slope of PV and the intercept at level 2, respectively; and PV is a set of phenological variables. In this study, DAS, DOY, GDD, and EAT were selected to assess phenological progress. In addition, we analyzed the applicability of UAV platforms to evaluate their potential and stability.

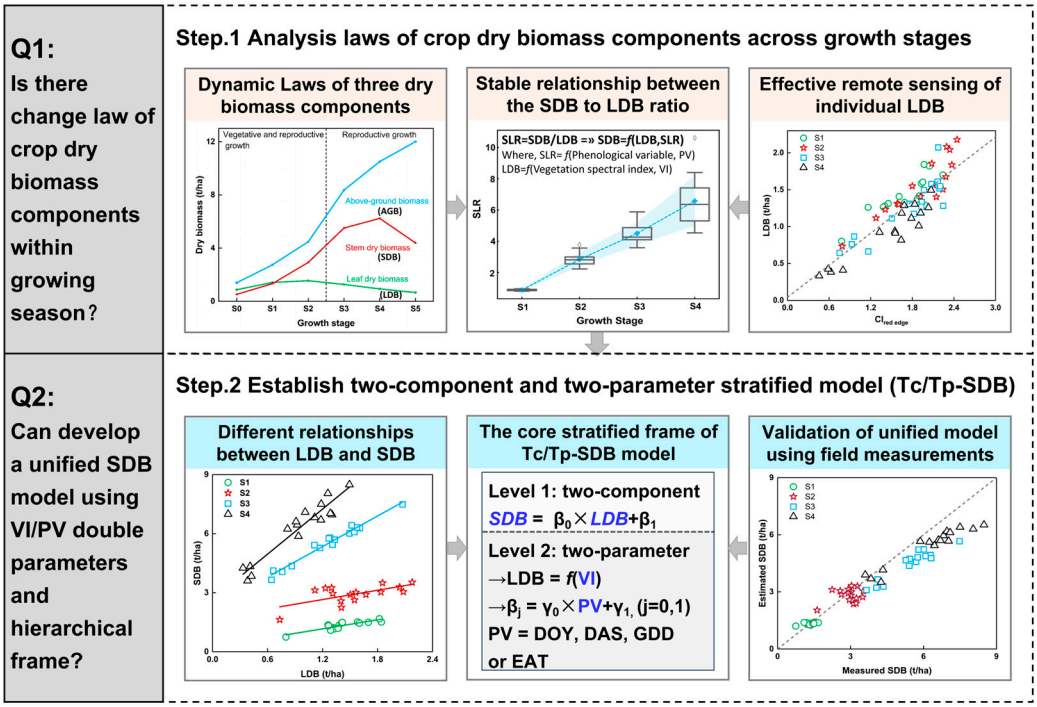

Figure 4. Flowchart of the approach used to develop and validate the Tc/Tp-SDB model.

2.5. Model Evaluation

The Pearson correlation coefficient (r) was used to analyze the linear relationship between different parameters in this study. The root mean square error (RMSE), Mean Absolute Error (MAE) and distance between indices of simulation and observation (DISO) were used to evaluate the general performance of the model [48]. DISO is a recently developed statistical index that describes the comprehensive performance of a model. Smaller values of MAE, DISO, and RMSE generally indicate greater accuracy and better performance of the model. These statistical indices were calculated as follows:

$$r = \frac{\sum_{i=1}^{n}(y_i - \overline{y})(x_i - \overline{x})}{\sqrt{\sum_{i=1}^{n}(y_i - \overline{y})^2 \sum_{i=1}^{n}(x_i - \overline{x})^2}} \tag{8}$$

$$RMSE = \sqrt{\frac{\sum_{i=1}^{n}(y_i - x_i)^2}{n}} \tag{9}$$

$$MAE = \frac{\sum_{i=1}^{n}|y_i - x_i|}{n} \tag{10}$$

$$DISO = \sqrt{(r-1)^2 + \left(\frac{RMSE}{\overline{x}}\right)^2 + \left(\frac{AE}{\overline{x}}\right)^2} \quad (11)$$

where x_i and y_i are the measured and estimated values, respectively; $\overline{x}$ and $\overline{y}$ are the average measured and estimated values, respectively; n is the total number of samples; and AE is the average error.

3. Results

3.1. Dry Biomass Statistics and Their Relationship with VIs

3.1.1. Dry Biomass Statistics

Figure 5 summarizes the changes in dry biomass for the four experiments. The results reveal that SDB exhibited an increasing trend from the jointing to flowering stages. From the jointing to filling stages, SDB stabilized or even decreased, perhaps due to plant senescence and the transfer of crop dry matter to the reproductive growth organ during the later growth stages of winter wheat. Furthermore, the range of LDB changes was relatively small during the four growing stages compared with SDB. This indicates that LDB may not be affected by crop stage development. Leaf biomass typically peaks during the flag-picking or flowering stage.

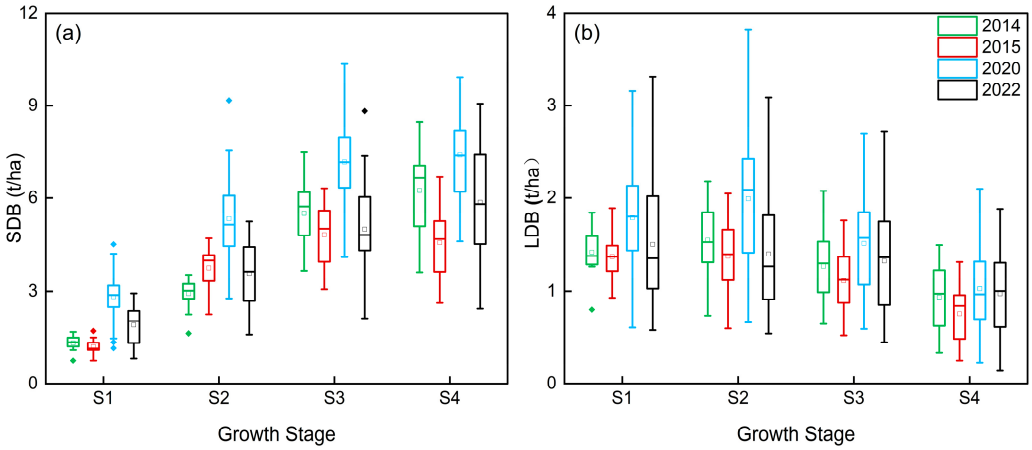

Figure 5. Winter wheat data collected in this study at different growth stages during the four-year experiment: (**a**) SDB, (**b**) LDB.

3.1.2. Relationship Between Different Types of VIs and PV and Dry Biomass

This study aims to construct a new two-component, two-parameter stratified estimate model for SDB that is suitable for all growth stages. Therefore, we analyzed the relationship between different typical vegetation indices (e.g., $CI_{\text{red edge}}$ and ND_{LMA}) and dry biomass at different growth stages (Figure 6). Data from the 2019–2020 growing season were used for the analysis, involving a single species with no irrigation gradient treatment (Figure 1d). All VIs were generally highly correlated with SDB and LDB ($r > 0.5$) at different growth stages. Compared with dry matter indices, chlorophyll indices showed a higher correlation with dry biomass at different growth stages, suggesting that these vegetation indices are a better choice for biomass estimation.

For LDB, leaf biomass was less affected by phenological growth stages ($r(S1-S4) > 0.65$). Thus, it was not necessary to consider the effect of phenology when constructing the VI-LDB method. In addition, SDB exhibited a linear relationship with the VIs at different growth stages. Consequently, the influence of phenology was considered when using remote sensing technology to estimate SDB. The measurements were made vertically, and thus the contribution of the winter wheat stem components to the overall canopy spectrum was small. For SDB, this high indirect correlation between VI and stem dry biomass was principally caused by the strong correlation between SDB and LDB at the canopy scale (Figure 7). Moreover, compared with the correlation between the

vegetation index and SDB (Figure 6a), the correlation between SDB and LDB (Figure 7c) was higher. Therefore, directly using VIs determined from spectra measured in the vertical direction may not accurately estimate the canopy stem dry biomass. These results reveal the ability of the stratified model established using PV and LDB to accurately predict SDB. Moreover, we used an extended Fourier amplitude sensitivity test (EFAST) to estimate the contribution of $CI_{red\ edge}$ and EAT to dry biomass. Further details of the data calculation can be found in Zhao et al. and Feng et al. [25,49]. The results (Table 3) show that the sensitivity indices of the EAT to SDB are greater than those of $CI_{red\ edge}$. Therefore, the influence of phenology cannot be ignored when estimating winter wheat stem biomass.

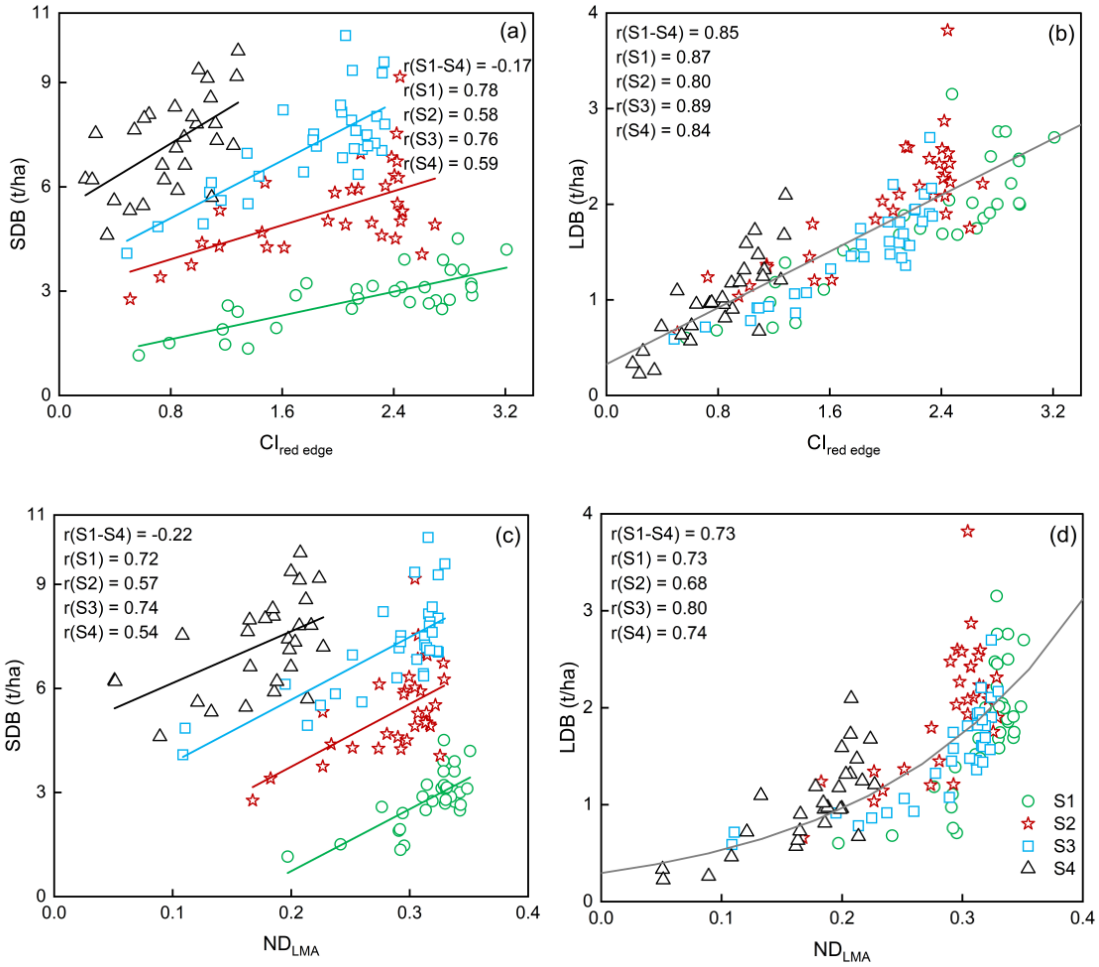

Figure 6. Relationship between VIs and dry biomass variables at different stages of the 2019–2020 growing season. (**a**) SDB vs. $CI_{red\ edge}$, (**b**) LDB vs. $CI_{red\ edge}$, (**c**) SDB vs. ND_{LMA}, (**d**) LDB vs. ND_{LMA}.

Table 3. Sensitivity indices of $CI_{red\ edge}$ and EAT to SDB and LDB.

Dry Biomass	Sensitivity Index		
	$CI_{red\ edge}$	EAT	Interaction
LDB	0.9810	0.0148	0.0042
SDB	0.1970	0.7066	0.0964

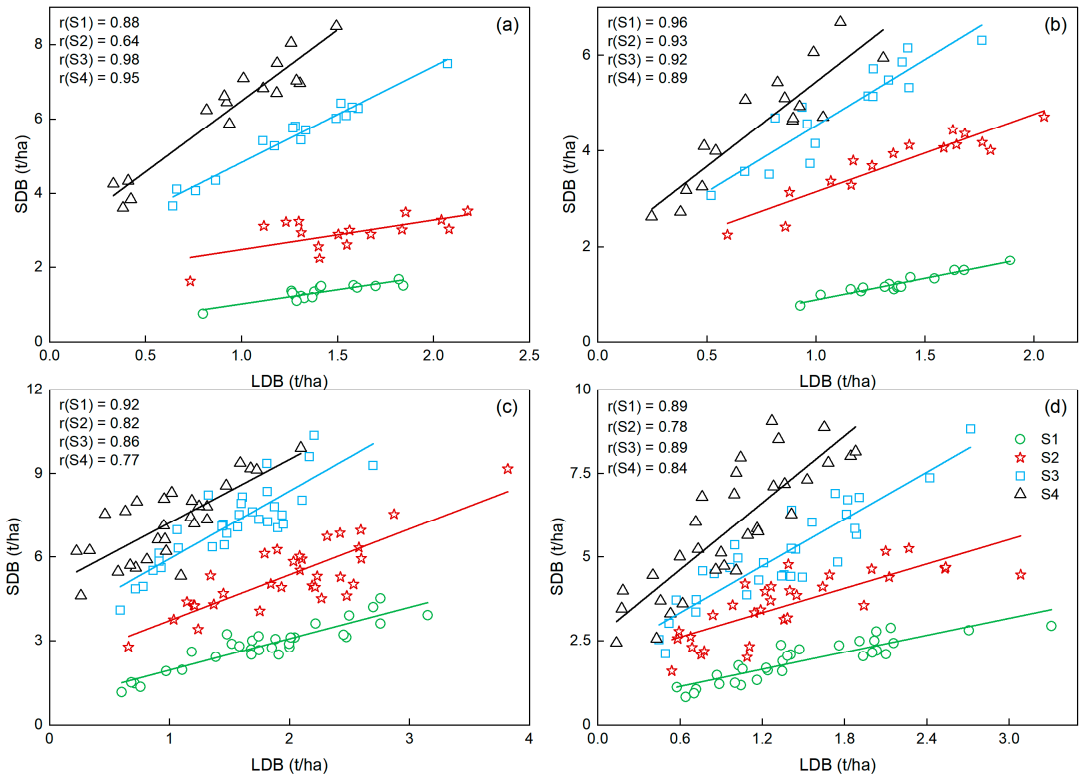

Figure 7. Relationship between LDB and SDB at different stages during four growing seasons: (**a**) 2013–2014, (**b**) 2014–2015, (**c**) 2019–2020, (**d**) 2021–2022.

3.1.3. Relationship Between LDB and SDB Changes with Phenology

To further understand the relationship between LDB and SDB, we determined their correlation at different growth stages during the four growing seasons (Figure 7). Strong and stable linear correlations (r > 0.60) were observed between LDB and SDB under different growth stages in all the experiments. For example, the correlations between LDB and SDB were significant ($p < 0.01$, r = 0.96, 0.93, 0.92, and 0.89) at different growth stages in the 2014–2015 growing season. However, the linear relationship between LDB and SDB in a specific growth stage could not accurately estimate SDB in other growth stages. As the growth stages progressed, the coefficients β_0 and β_1 in Equation (4) showed an increasing trend. This proves that the relationship between stem biomass and leaf biomass is highly related to phenology. Therefore, it is key and a base for establishing a phenologically constrained hierarchical model to explore the relationship between coefficients and PV across different experiments.

3.2. Results of Leaf Dry Biomass Estimation

Next, LDB-sensitive VIs were selected by 5-fold cross-validation for all growth stages across four planting seasons. We calculated the average (μ) and standard deviation (σ) of the r, RMSE, MAE, and DISO from the test datasets of the six vegetation indices. In general, vegetation indices related to chlorophyll performed better than those related to dry matter for LDB estimation. This indicates that chlorophyll indices are more suitable for estimating leaf biomass. Moreover, the results (Figure 8) show that the LDB estimated with $CI_{red\ edge}$ (r = 0.81 ± 0.03, RMSE = 0.33 ± 0.06 t/ha, MAE = 0.25 ± 0.02 t/ha, DISO = 0.31 ± 0.03) was more accurate than that estimated by other vegetation indices. Therefore, $CI_{red\ edge}$ was used for subsequent modeling.

$CI_{red\ edge}$ was used to develop the VI-LDB method in this study (Figure 9). Data from Exp. 1 and Exp. 4 were employed to calibrate the model, while the datasets from Exp. 2 and Exp. 3 were used to estimate model accuracy. The results of these

calculations demonstrate the performance of the $CI_{red\ edge}$-LDB method on the calibration (r = 0.86, RMSE = 0.28 t/ha, MAE = 0.21 t/ha, DISO = 0.25) and validation (r = 0.83, RMSE = 0.42 t/ha, MAE = 0.30 t/ha, DISO = 0.36) datasets. In general, the estimated accuracy of leaf biomass fluctuates slightly in calibration and validation (Table 4). Notably, LDB was underestimated when the measured LDB exceeded 2.00 t/ha (Figure 9a,b). A similar conclusion can be obtained by analyzing the residual distribution plot (Figure 9c,d). The larger residuals (μ = 0.58 and σ = 0.38) generally occurred when the measured LDB was greater than 2.00 t/ha. Therefore, the phenomenon of LDB underestimation may be attributed to the impact of the vegetation index and the limited number of calibrated samples with measured LDB greater than 2.00 t/ha. These factors may increase the magnitude of fluctuations in estimates obtained by the $CI_{red\ edge}$-LDB method.

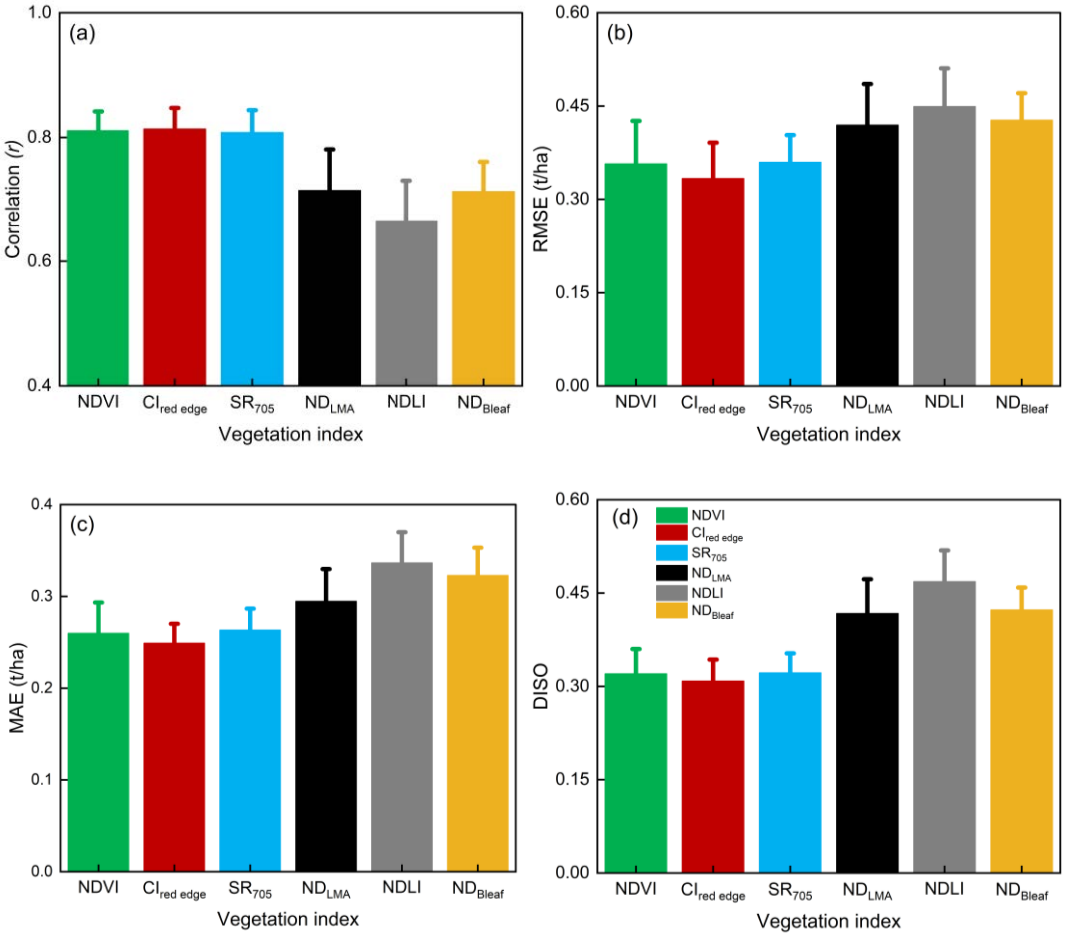

Figure 8. Average and standard deviation of the correlation coefficient r (**a**), RMSE (**b**), MAE (**c**), and DISO (**d**) using the test datasets from the 5-fold cross-validation.

Table 4. The accuracy indices summary of the different growth stages of the estimated LDB from the $CI_{red\ edge}$-LDB method.

Dataset	Indices (t/ha)	Growth Stages			
		S1	S2	S3	S4
Calibration	RMSE	0.32	0.25	0.31	0.20
	MAE	0.25	0.19	0.25	0.17
Validation	RMSE	0.39	0.59	0.31	0.33
	MAE	0.29	0.44	0.23	0.25
All datasets	RMSE	0.36	0.46	0.31	0.27
	MAE	0.27	0.31	0.24	0.21

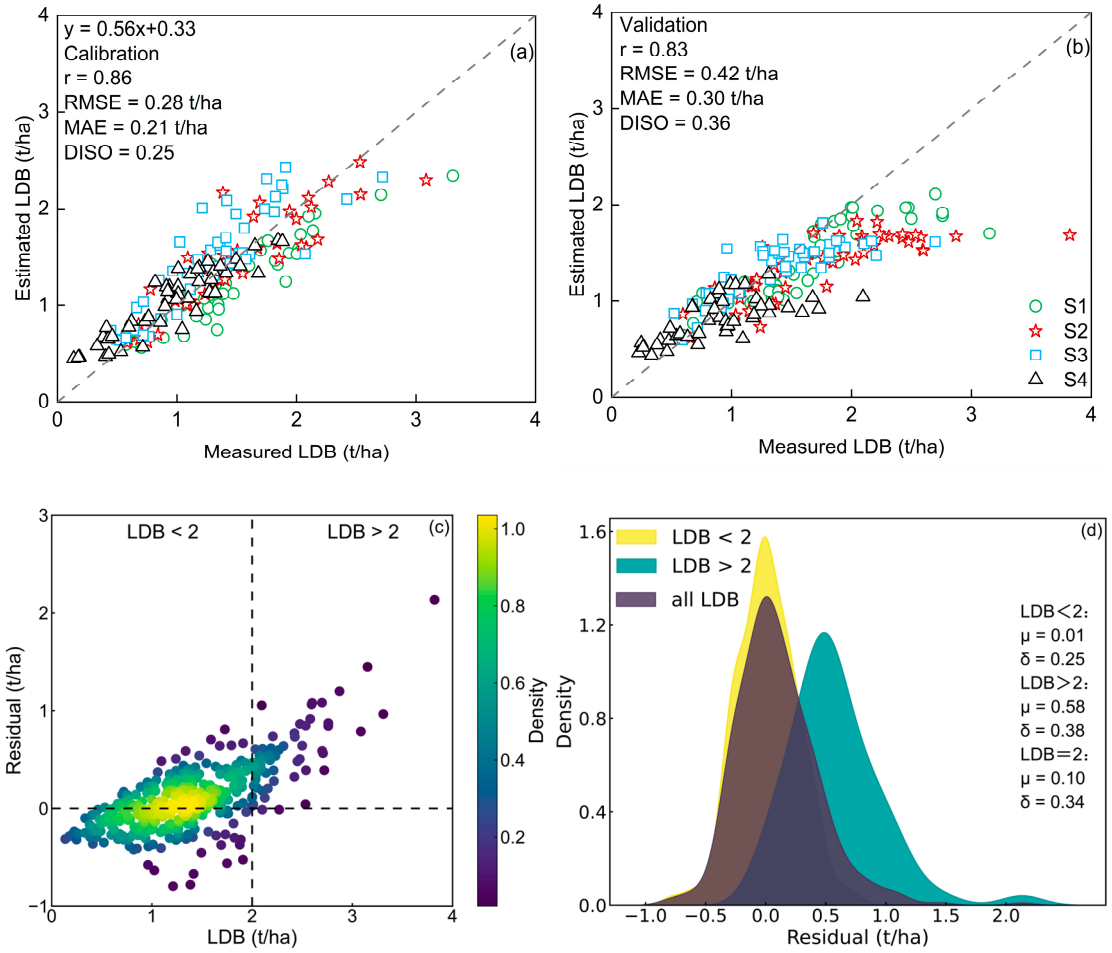

Figure 9. Relationship (**a**,**b**) between measured and estimated LDB using the CIred edge-LDB method, and the residual distributions between different LDB levels (**c**,**d**).

3.3. Stem Dry Biomass Estimations with the Tc/Tp-SDB Model

3.3.1. Estimated SDB with Different PVs

The results in Section 3.1.3 showed that the correlation coefficient between SDB and LDB strengthened as the growth stage progressed. To accurately establish the Tc/Tp-SDB model, we analyzed the relationship between coefficients β_0 and β_1 and phenological variables using the calibration datasets. For this analysis, the LDB was estimated with the $CI_{red\ edge}$-LDB method. Table 5 shows the linear relationships between the coefficients and phenological variables, which aided in estimating SDB using remote sensing-based approaches. The r values between coefficient β_0 and different PVs were all greater than 0.80 and highly significant ($p < 0.01$). In addition, all PV values were significantly correlated with β_1, particularly DOY and DAS, with r values greater than 0.50. These served as a theoretical basis for the development of the Tc/Tp-SDB model. Accordingly, we constructed the Tc/Tp-SDB model for different growth stages to estimate SDB using different PV values as constraints.

The Tc/Tp-SDB models were divided into temporal (DOY, DAS) and thermal (GDD, EAT) models based on constraint types, and the calibration datasets were used to test the performance of these models (Figure 10). EAT and DAS can be calculated as DAS and DOY plus fixed values, respectively. However, there were differences in the performance of the two model types on the calibration datasets. Therefore, we selected the optimal modeling methods for each type. For the temporal metrics, Tc/Tp-SDB-EAT (r = 0.92, RMSE = 0.82 t/ha, MAE = 0.64 t/ha, DISO = 0.22) performed better than Tc/Tp-SDB-GDD (r = 0.91, RMSE = 0.86 t/ha, MAE = 0.68 t/ha, DISO = 0.23). For the thermal metrics,

Tc/Tp-SDB, Tc/Tp-SDB-DOY (r = 0.90, RMSE = 0.92 t/ha, MAE = 0.69 t/ha, DISO = 0.25) performed better than Tc/Tp-SDB-DAS (r = 0.87, RMSE = 1.01 t/ha, MAE = 0.84 t/ha, DISO = 0.30). Based on these results, EAT and DOY were selected as the constraint variables to establish the Tc/Tp-SDB-EAT and Tc/Tp-SDB-DOY models, respectively.

Table 5. Stem dry biomass stratified model constrained by different PV values. Note: ** represents a significant level at 0.01.

Phenological Variables	Coefficient	Model	r
GDD	β_0	$\beta_0 = 0.004GDD - 0.64$	0.96 **
	β_1	$\beta_1 = 0.001GDD + 0.91$	0.34 **
EAT	β_0	$\beta_0 = 0.005EAT - 2.94$	0.95 **
	β_1	$\beta_1 = 0.001EAT + 0.51$	0.37 **
DOY	β_0	$\beta_0 = 0.08DOY - 7.86$	0.89 **
	β_1	$\beta_1 = 0.02DOY - 1.17$	0.54 **
DAS	β_0	$\beta_0 = 0.07DAS - 13.69$	0.84 **
	β_1	$\beta_1 = 0.02DAS - 3.16$	0.59 **

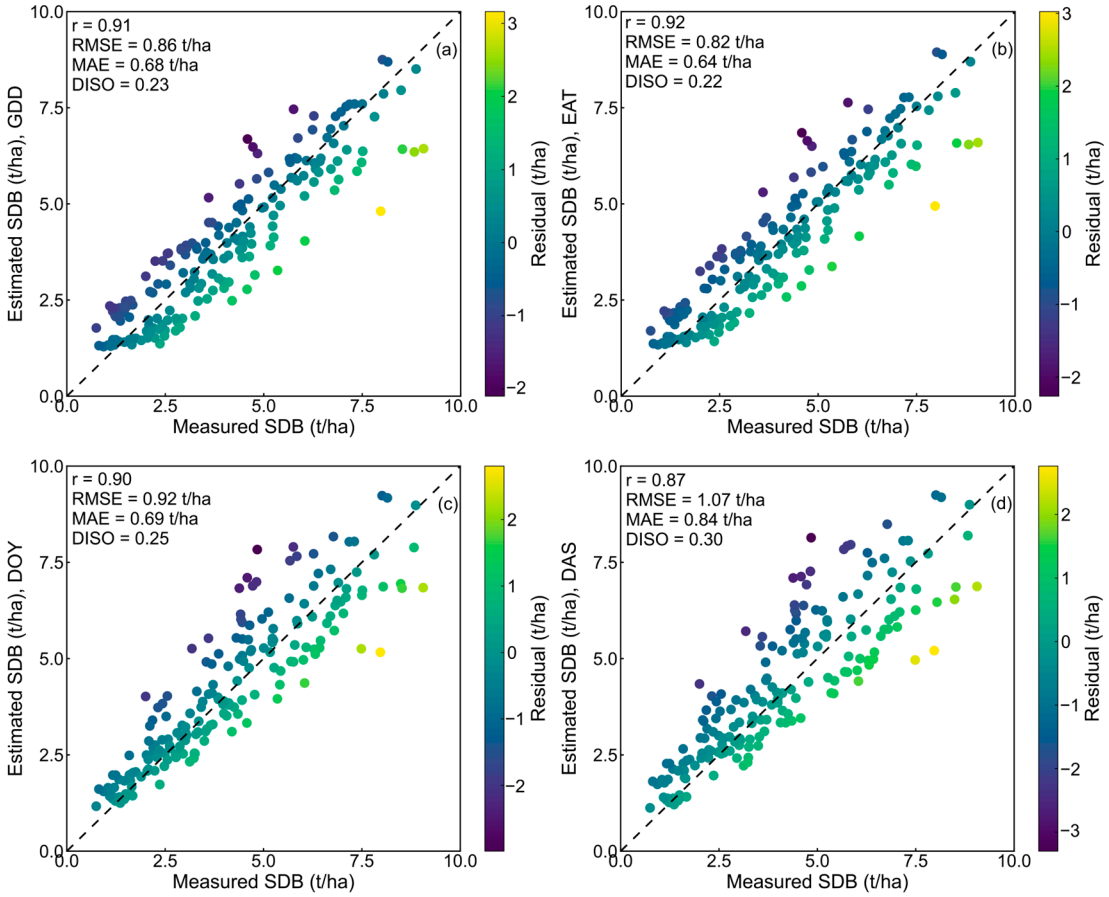

Figure 10. Relationship between the measured and estimated SDB of winter wheat using the calibration datasets. (**a**) GDD; (**b**) EAT; (**c**) DOY; (**d**) DAS.

3.3.2. Validation of the Tc/Tp-SDB Model Based on the Optimal PV

Figure 11a,b presents the relationship between the measured and estimated SDB using the validation datasets for Tc/Tp-SDB-EAT and Tc/Tp-SDB-DOY. Both models were established using the same calibration and validation datasets. Tc/Tp-SDB-EAT (r = 0.85, RMSE = 1.28 t/ha, MAE = 0.95 t/ha, DISO = 0.31) and Tc/Tp-SDB-DOY (r = 0.85, RMSE = 1.36 t/ha, MAE = 1.03 t/ha, DISO = 0.34) performed well with the validation

datasets. Further analysis of the distributions of residual values (Figure 11c,d) revealed that both models exhibited the same trend regarding changes in estimates. Notably, SDB was significantly underestimated when the measured SDB was greater than 6.00 t/ha, especially for Tc/Tp-SDB-DOY. Moreover, we also calculated the error distribution of the different growth stages of the estimated SDB from the Tc/Tp-SDB-EAT model. During the entire growing season, stem biomass generally showed an increasing trend (Figure 5a). The estimation error (Table 6) of stem biomass also increased with the progress of the growth stages and reached the maximum (all datasets: RMSE = 1.36 t/ha, MAE = 1.08 t/ha) during the filling stage. Generally, RMSE and MAE values were also related to the range of datasets. In summary, these models accurately predicted the SDB at important growth stages of winter wheat using vegetation indices and phenological variables.

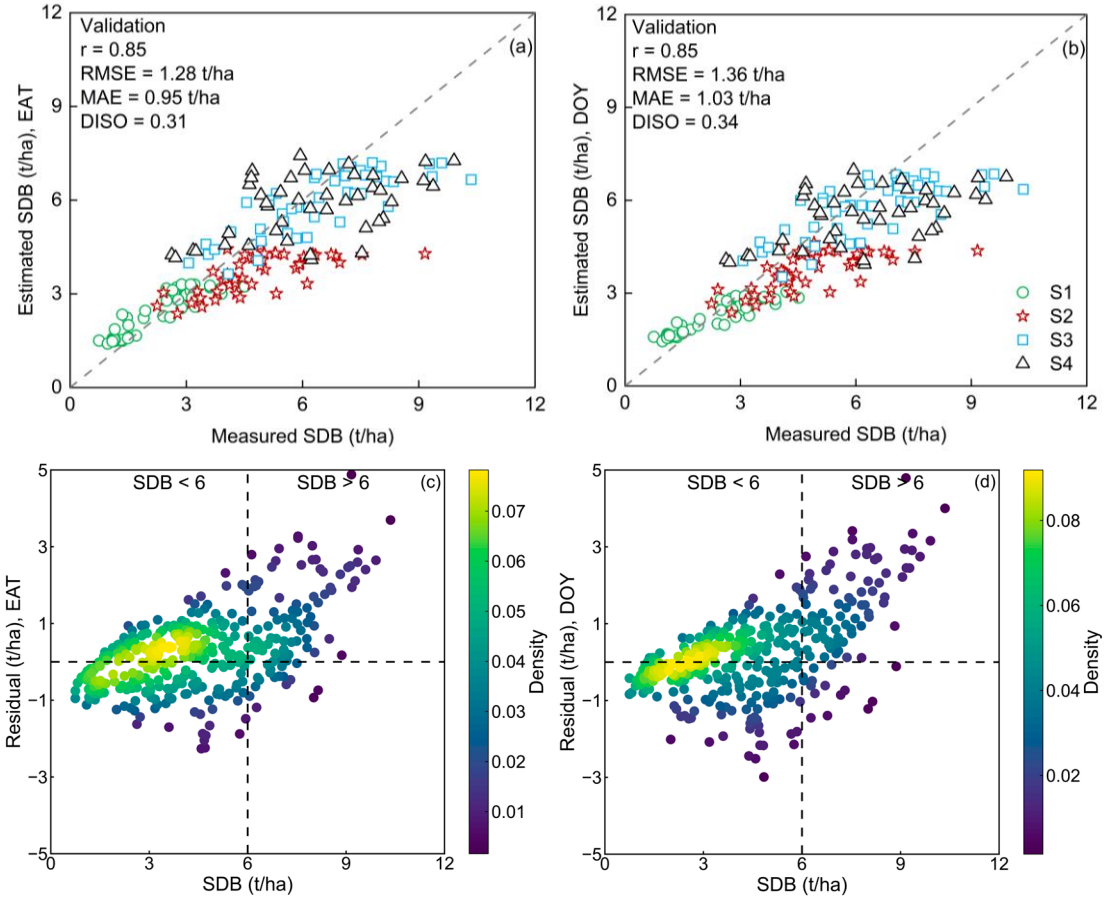

Figure 11. Relationship (**a**,**b**) between the measured and estimated SDB of winter wheat using the validation datasets, and the residual distribution for the Tc/Tp-SDB-EAT and Tc/Tp-SDB-DOY models under different SDB levels (**c**,**d**).

Table 6. The accuracy indices summary of the different growth stages of the estimated SDB from the Tc/Tp-SDB-EAT model.

Dataset	Indices (t/ha)	Growth Stages			
		S1	S2	S3	S4
Calibration	RMSE	0.61	0.74	0.79	1.07
	MAE	0.53	0.63	0.60	0.81
Validation	RMSE	0.48	1.55	1.17	1.61
	MAE	0.40	1.21	0.89	1.37
All datasets	RMSE	0.55	1.21	1.00	1.36
	MAE	0.46	0.92	0.74	1.08

3.3.3. Validation of the Tc/Tp-SDB Model with UAV Hyperspectral Images

We subsequently applied the Tc/Tp-SDB-EAT model to UAV hyperspectral images and determined the spatial distribution maps of the predicted SDB (Figure 12). The visualization results reveal that the SDB of winter wheat exhibited an increasing trend, consistent with the distribution of the ground survey data (Figure 5a), indicating that the model is highly suitable for UAV platforms. Therefore, the analysis of UAV hyperspectral images may be a convenient and useful method for estimating the growth of winter wheat stems.

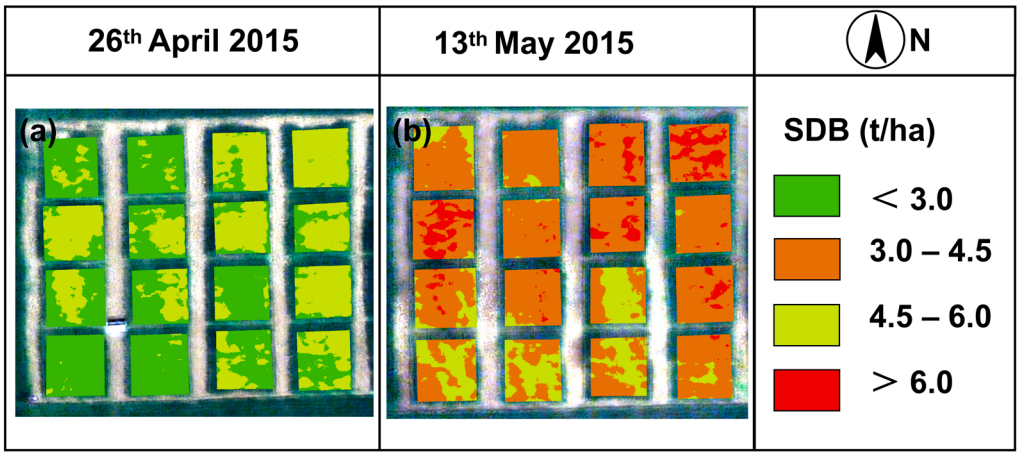

Figure 12. SDB maps determined from the Tc/Tp-SDB model with UAV hyperspectral images. (**a**) SDB during the flagging stage (26th April); (**b**) SDB during the flowering stage (13th May).

4. Discussion

4.1. Effect of LDB Estimation Accuracy on Tc/Tp-SDB Model Performance

LDB is a crucial intermediate variable in the Tc/Tp-SDB model. Accurate LDB estimation is a prerequisite for precise SDB estimation. Therefore, we examined the residual distribution of LDB and SDB at various growth stages, using EAT as input for the Tc/Tp-SDB model. The results show (Figure 13a) that the residuals of LDB remained relatively stable across all growth stages. This is likely due to the low sensitivity of leaf biomass to phenological changes. Our results support the findings of Zhao et al. and Yue et al. [25,26]. However, the residuals of the SDB exhibited a broader distribution at each stage, especially during the filling stage (Table 6). Since the SDB estimation model proposed in this study is based on LDB and phenological variables, this is evident from Equations (5)–(7). The two parameters, β_0 and β_1, derived from phenological regression analysis, can be interpreted as follows: β_0 can be viewed as the ratio of SDB to LDB (SLR) (undoubtedly, SDB = SLR $\times$ LDB), whereas β_1 may be construed as the error correction term for estimating SDB using LDB. From this perspective, inaccuracies in estimating LDB will lead to progressively increasing errors in estimating SDB as the crop's SLR varies across different growth stages (Figure 13b). Therefore, considering this standpoint, improving the accuracy of LDB estimates, especially if it is greater than 2.0 t/ha (Figure 9c), is crucial for achieving high-precision estimation of SDB. From the perspective of Tc/Tp-SDB model error propagation, if the SDB estimation accuracy is better than 80% (for example, SLR = 5.0, SDB = 5.0 t/ha), that is, when the maximal error is about 1.0 t/ha, the LDB error is required to be no less than 20%, as same as the maximal error of LDB should be less than 0.2 t/ha. In addition, new observation modes should be considered to improve the accuracy of estimation. Zhu et al. showed that integrating canopy structure information from LiDAR with vegetation indices enhances the accuracy of canopy biomass predictions [17].

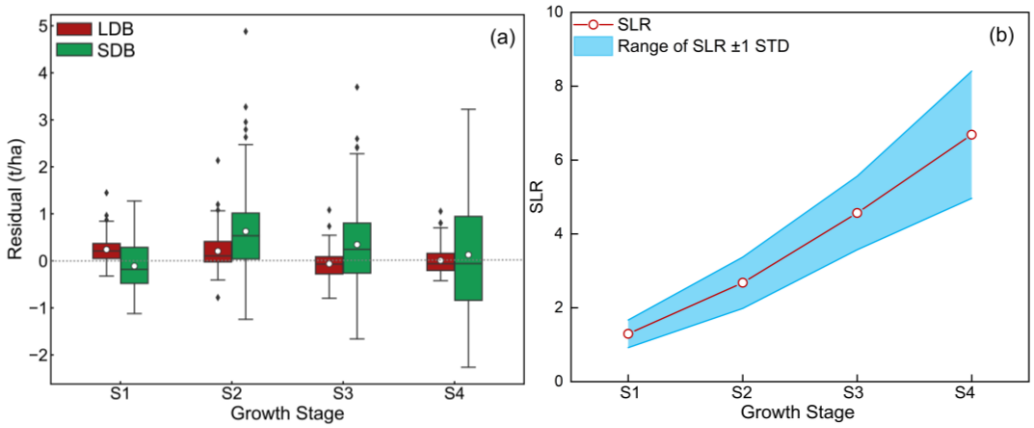

Figure 13. The distribution of the residuals of LDB and SDB in different growth stages (**a**), and the change of SLR with growth stage (**b**). Note: both (**a**,**b**) use all datasets.

4.2. Effect of Phenological Variables and VIs on Estimated SDB

To explore the effect of phenological variables and vegetation indices on estimated SDB, we employed linear regression models using only $CI_{red\ edge}$ and EAT for the SDB estimations. In addition, we compared the Tc/Tp-SDB-EAT model with these models to evaluate its performance. The single-parameter regression method is also commonly used to estimate SDB [31,50]. We obtained similar conclusions to the sensitivity analysis (Table 3). Figure 14 shows that the model using only EAT (r = 0.71, RMSE = 1.62 t/ha, MAE = 1.26 t/ha, DISO = 0.45) outperformed the $CI_{red\ edge}$-based model (r = 0.03, RMSE = 2.44 t/ha, MAE = 1.99 t/ha, DISO = 1.10) for the validation datasets. However, the performance of these models demonstrates that they are not the most suitable choice for actual agricultural production environments.

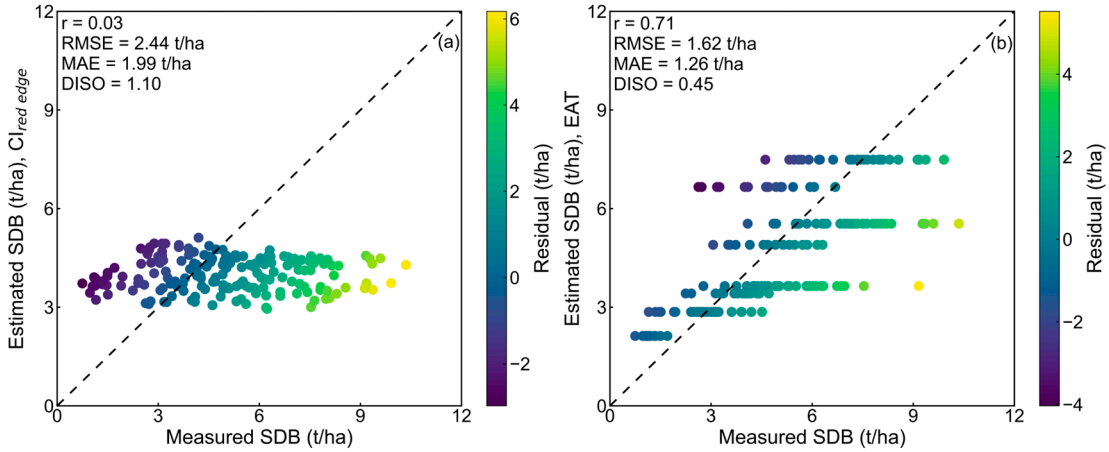

Figure 14. Relationship between the measured and estimated SDB of winter wheat using the validation datasets with models using only (**a**) $CI_{red\ edge}$, (**b**) EAT.

Crop biomass accumulation is closely related to phenology. In the early and middle stages of crop growth, biomass accumulation increased continuously [51,52]. Jungers et al. analyzed the relationship between intermediate wheatgrass biomass and GDD and established an empirical model to predict crop height and dry biomass [53]. In theory, there is a positive correlation between dry biomass and phenological variables during the same planting season. Notably, the phenological variables in our study are ordered and continuous parameters [49,54]. Due to the spatial resolution of ERA5, the experimental area had only one phenological variable for each growth stage. Therefore, the estimated SDB had only one estimation result for each growth stage. However, the estimated value could represent the average dry biomass of winter wheat. Moreover, we argue that it is possible to achieve accurate estimations for large-scale areas of SDB using only phenological variables.

VIs are strongly correlated with the crop canopy structure [55,56]. Consequently, VIs may also indicate the development process and demonstrate differences in experimental planting plots. The winter wheat growth represented by VIs does not typically change in a linear manner throughout the whole growth stage. For example, the NDVI curve of winter wheat typically exhibits two peaks and one valley [57,58]. The stem dry biomass measured in our experiment increased gradually, which differed from the change trends of the VIs. Therefore, the models considering only phenological variables outperformed VI-based models. Zhao et al. reported the difficulties in accurately predicting winter wheat AGB using only OSAVI without considering phenology as a constraint [25]. This also demonstrates the importance of meteorological factors for estimating biomass. In summary, combining VIs and phenological variables facilitates the accurate prediction of SDB.

4.3. Limitations and Future Prospects

The estimation of crop dry biomass using proximal hyperspectral data plays an important role in agricultural monitoring. The model developed in our study achieved promising results in estimating stem biomass for different years and growth stages. Moreover, our model exhibited excellent robustness and good applicability for UAV platforms. However, despite the progress made by this study, several issues require further exploration.

First, estimating leaf biomass using canopy spectra still faces significant challenges. Our results indicate that LDB estimations had a marked impact on the Tc/Tp-SDB model. The canopy structure changes greatly as the growth stage progresses. Soil background, spectral saturation, and the number of wheat ears all increase the uncertainty in LDB estimations [59]. Li et al. developed practical semi-empirical models based on optimal wavelet features to predict leaf water content from canopy hyperspectral reflectance data, demonstrating the application of canopy spectra to accurately estimate LDB [60]. Moreover, due to the ability of machine learning to utilize multiple spectral features, the effect of spectral saturation on biomass estimation can also be reduced using this method [61,62].

Second, the easy access to phenological variables is key to the success of the model in large-scale SDB estimation. However, DAS heavily relies on manual recording, which is not conducive to large-scale remote sensing biomass estimation. Compared with DAS and EAT, DOY and GDD data are easier to obtain without the need for field observations and recordings. As core parameters of Tc/Tp-SDB, DOY or GDD could be used in large-scale applications. Moreover, Zhu et al. found that the relationship between LDB and SDB is affected by genotype, environment, and management [63]. Therefore, future work is likely to consider the construction of a comprehensive indicator to replace the phenological variables in our model.

Third, the proposed Tc/Tp-SDB model was only used for estimating winter wheat SDB. The robustness and compatibility of this model require further exploration with other crops, such as paddy rice and maize. Cheng et al. found that the relationship between paddy rice stems and leaves changes with growth stage, similar to that of winter wheat [27]. Therefore, the parameters need to be recalibrated when applying our model to other crops. Furthermore, stem biomass is the primary phenotype indicating the quality of silage crop varieties. Calibration of the model to estimate the stem biomass of silage crops is also a priority for future research.

Finally, the scale effects of the Tc/Tp-SDB model, a common problem in large-scale remote sensing applications of crop biomass, require further consideration. We demonstrated that Tc/Tp-SDB is suitable for data collected using proximal sensors. Large-scale study areas are a key issue for future research. Future work will focus on the extended application of the Tc/Tp-SDB model to estimate winter wheat dry and fresh stem biomass at the satellite scale, with the aim of further exploring the universality of the Tc/Tp-SDB model.

5. Conclusions

This study demonstrated the ability of the two-component and two-parameter stratified model (Tc/Tp-SDB) to accurately estimate winter wheat SDB across growth stages.

Based on the results, the following conclusions were drawn: (1) With the advancement of the growth stage, the coefficients of the linear regression models between LDB and SDB exhibited an increasing trend. Moreover, the values of coefficients β_0 and β_1 exhibited a stable linear relationship with the PVs. (2) Vegetation index is one of the important parameters of the Tc/Tp-SDB model. Compared with dry matter indices, selecting vegetation indices related to chlorophyll as the input of the model yielded more accurate SDB estimations. (3) The Tc/Tp-SDB models were tested under different phenological constraints. The Tc/Tp-SDB-EAT model performed well for winter wheat SDB predictions, with r, RMSE, MAE, and DISO values of 0.85, 1.28 t/ha, 0.95 t/ha, and 0.31, respectively, for the validation datasets. Tc/Tp-SDB outperformed other empirical models for SDB estimation. Moreover, the proposed model showed good potential for estimating SDB from UAV hyperspectral imagery. In conclusion, the established Tc/Tp-SDB model can be used to accurately estimate winter wheat stem biomass, which has practical implications for local and global smart agricultural production employing ecological utilization of stalks, carbon cycle monitoring, and the assessment of biomass energy.

Author Contributions: W.C.: Conceptualization, Methodology, Data curation, Software, Writing—original draft. G.Y.: Methodology, Review and editing, Resources, Funding acquisition, Project administration. Y.M.: Conceptualization, Investigation. H.F.: Investigation, Review and editing, Validation. H.L.: Validation, Visualization. A.T.: Software, Resources, Visualization. J.Z.: Formal analysis, Software. X.X. and H.Y.: Data curation, Supervision. C.L.: Investigation, Methodology, Review and editing. Z.L.: Supervision, Validation. All authors have read and agreed to the published version of the manuscript.

Funding: This research was supported by grants from the National Key Research and Development Program of China (2023YFD2000100), the Ningxia Hui Autonomous Region Key Research and Development (2023BEG02050), and the National Natural Science Foundation of China (42171303).

Data Availability Statement: The raw data of field measurements are available from the corresponding author, G.Y., upon reasonable request.

Acknowledgments: We thank the Information Technology Research Center, Beijing Academy of Agriculture and Forestry Sciences for providing the experimental base. We are grateful to the editors and anonymous reviewers for their constructive and helpful comments, which improved the quality of this paper.

Conflicts of Interest: The authors declare that they have no known competing financial interests or personal relationships that could have appeared to influence the work reported in this paper.

References

1. Fei, S.; Xu, D.; Chen, Z.; Xiao, Y.; Ma, Y. MLR-Based Feature Splitting Regression for Estimating Plant Traits Using High-Dimensional Hyperspectral Reflectance Data. *Field Crops Res.* **2023**, *293*, 108855. [CrossRef]
2. Reynolds, M.P.; Braun, H.-J. Wheat Improvement. In *Wheat Improvement*; Reynolds, M.P., Braun, H.-J., Eds.; Springer International Publishing: Cham, Switzerland, 2022; pp. 3–15, ISBN 978-3-030-90672-6.
3. Weiss, M.; Jacob, F.; Duveiller, G. Remote Sensing for Agricultural Applications: A Meta-Review. *Remote Sens. Environ.* **2020**, *236*, 111402. [CrossRef]
4. Gupta, M.L.; Pradhan, K. Chemical and Biological Evaluation of Ensiled Wheat Straw. *J. Dairy Sci.* **1977**, *60*, 1088–1094. [CrossRef]
5. Liu, J.; Fang, L.; Qiu, T.; Chen, J.; Wang, H.; Liu, M.; Yi, J.; Zhang, H.; Wang, C.; Sardans, J.; et al. Crop Residue Return Achieves Environmental Mitigation and Enhances Grain Yield: A Global Meta-Analysis. *Agron. Sustain. Dev.* **2023**, *43*, 78. [CrossRef]
6. Chang, Z.; Fan, L.; Wigneron, J.-P.; Wang, Y.-P.; Ciais, P.; Chave, J.; Fensholt, R.; Chen, J.M.; Yuan, W.; Ju, W.; et al. Estimating Aboveground Carbon Dynamic of China Using Optical and Microwave Remote-Sensing Datasets from 2013 to 2019. *J. Remote Sens.* **2023**, *3*, 0005. [CrossRef]
7. Wocher, M.; Berger, K.; Verrelst, J.; Hank, T. Retrieval of Carbon Content and Biomass from Hyperspectral Imagery over Cultivated Areas. *ISPRS J. Photogramm. Remote Sens.* **2022**, *193*, 104–114. [CrossRef]
8. Shu, M.; Shen, M.; Dong, Q.; Yang, X.; Li, B.; Ma, Y. Estimating the Maize Above-Ground Biomass by Constructing the Tridimensional Concept Model Based on UAV-Based Digital and Multi-Spectral Images. *Field Crops Res.* **2022**, *282*, 108491. [CrossRef]

9. Zhu, Y.; Liu, J.; Tao, X.; Su, X.; Li, W.; Zha, H.; Wu, W.; Li, X. A Three-Dimensional Conceptual Model for Estimating the Above-Ground Biomass of Winter Wheat Using Digital and Multispectral Unmanned Aerial Vehicle Images at Various Growth Stages. *Remote Sens.* **2023**, *15*, 3332. [CrossRef]
10. Wang, L.; Zhou, X.; Zhu, X.; Dong, Z.; Guo, W. Estimation of Biomass in Wheat Using Random Forest Regression Algorithm and Remote Sensing Data. *Crop J.* **2016**, *4*, 212–219. [CrossRef]
11. Yang, G.; Liu, J.; Zhao, C.; Li, Z.; Huang, Y.; Yu, H.; Xu, B.; Yang, X.; Zhu, D.; Zhang, X.; et al. Unmanned Aerial Vehicle Remote Sensing for Field-Based Crop Phenotyping: Current Status and Perspectives. *Front. Plant Sci.* **2017**, *8*, 1111. [CrossRef]
12. Yu, D.; Zha, Y.; Sun, Z.; Li, J.; Jin, X.; Zhu, W.; Bian, J.; Ma, L.; Zeng, Y.; Su, Z. Deep Convolutional Neural Networks for Estimating Maize Above-Ground Biomass Using Multi-Source UAV Images: A Comparison with Traditional Machine Learning Algorithms. *Precis. Agric.* **2023**, *24*, 92–113. [CrossRef]
13. Liu, Y.; Feng, H.; Yue, J.; Jin, X.; Fan, Y.; Chen, R.; Bian, M.; Ma, Y.; Song, X.; Yang, G. Improved Potato AGB Estimates Based on UAV RGB and Hyperspectral Images. *Comput. Electron. Agric.* **2023**, *214*, 108260. [CrossRef]
14. Liu, Y.; Feng, H.; Yue, J.; Fan, Y.; Bian, M.; Ma, Y.; Jin, X.; Song, X.; Yang, G. Estimating Potato Above-Ground Biomass by Using Integrated Unmanned Aerial System-Based Optical, Structural, and Textural Canopy Measurements. *Comput. Electron. Agric.* **2023**, *213*, 108229. [CrossRef]
15. Teng, W.; Yu, Q.; Mischenko, I.C.; Rice, A.M.; Richardson, J.B. Predicting Foliar Nutrient Concentrations across Geologic Materials and Tree Genera in the Northeastern United States Using Spectral Reflectance and Partial Least Squares Regression Models. *J. Remote Sens.* **2024**, *4*, 0093. [CrossRef]
16. Jin, S.; Zhang, W.; Shao, J.; Wan, P.; Cheng, S.; Cai, S.; Yan, G.; Li, A. Estimation of Larch Growth at the Stem, Crown, and Branch Levels Using Ground-Based LiDAR Point Cloud. *J. Remote Sens.* **2022**, *2022*, 9836979. [CrossRef]
17. Zhu, Y.; Zhao, C.; Yang, H.; Yang, G.; Han, L.; Li, Z.; Feng, H.; Xu, B.; Wu, J.; Lei, L. Estimation of Maize Above-Ground Biomass Based on Stem-Leaf Separation Strategy Integrated with LiDAR and Optical Remote Sensing Data. *PeerJ* **2019**, *7*, e7593. [CrossRef]
18. Liu, Y.; Wang, B.; Sheng, Q.; Li, J.; Zhao, H.; Wang, S.; Liu, X.; He, H. Dual-Polarization SAR Rice Growth Model: A Modeling Approach for Monitoring Plant Height by Combining Crop Growth Patterns with Spatiotemporal SAR Data. *Comput. Electron. Agric.* **2023**, *215*, 108358. [CrossRef]
19. Yang, H.; Yang, G.; Gaulton, R.; Zhao, C.; Li, Z.; Taylor, J.; Wicks, D.; Minchella, A.; Chen, E.; Yang, X. In-Season Biomass Estimation of Oilseed Rape (*Brassica napus* L.) Using Fully Polarimetric SAR Imagery. *Precis. Agric.* **2019**, *20*, 630–648. [CrossRef]
20. Sun, Q.; Chen, L.; Zhang, B.; Qu, X.; Cui, Y.; Shu, M.; Gu, X. Evaluation of Growth Recovery Grade in Lodging Maize via UAV-Based Hyperspectral Images. *J. Remote Sens.* **2024**, *4*, 0253. [CrossRef]
21. Fei, S.; Xiao, S.; Li, Q.; Shu, M.; Zhai, W.; Xiao, Y.; Chen, Z.; Yu, H.; Ma, Y. Enhancing Leaf Area Index and Biomass Estimation in Maize with Feature Augmentation from Unmanned Aerial Vehicle-Based Nadir and Cross-Circling Oblique Photography. *Comput. Electron. Agric.* **2023**, *215*, 108462. [CrossRef]
22. Yang, G.; Zhao, C.; Liu, Q.; Huang, W.; Wang, J. Inversion of a Radiative Transfer Model for Estimating Forest LAI From Multisource and Multiangular Optical Remote Sensing Data. *IEEE Trans. Geosci. Remote Sens.* **2011**, *49*, 988–1000. [CrossRef]
23. Zhao, C.; Li, H.; Li, P.; Yang, G.; Gu, X.; Lan, Y. Effect of Vertical Distribution of Crop Structure and Biochemical Parameters of Winter Wheat on Canopy Reflectance Characteristics and Spectral Indices. *IEEE Trans. Geosci. Remote Sens.* **2017**, *55*, 236–247. [CrossRef]
24. Wang, L.; Hunt, E.R.; Qu, J.J.; Hao, X.; Daughtry, C.S.T. Towards Estimation of Canopy Foliar Biomass with Spectral Reflectance Measurements. *Remote Sens. Environ.* **2011**, *115*, 836–840. [CrossRef]
25. Zhao, Y.; Meng, Y.; Han, S.; Feng, H.; Yang, G.; Li, Z. Should Phenological Information Be Applied to Predict Agronomic Traits across Growth Stages of Winter Wheat? *Crop J.* **2022**, *10*, 1346–1352. [CrossRef]
26. Yue, J.; Yang, H.; Yang, G.; Fu, Y.; Wang, H.; Zhou, C. Estimating Vertically Growing Crop Above-Ground Biomass Based on UAV Remote Sensing. *Comput. Electron. Agric.* **2023**, *205*, 107627. [CrossRef]
27. Cheng, T.; Song, R.; Li, D.; Zhou, K.; Zheng, H.; Yao, X.; Tian, Y.; Cao, W.; Zhu, Y. Spectroscopic Estimation of Biomass in Canopy Components of Paddy Rice Using Dry Matter and Chlorophyll Indices. *Remote Sens.* **2017**, *9*, 319. [CrossRef]
28. Zhao, D.; Yang, H.; Yang, G.; Yu, F.; Zhang, C.; Chen, R.; Tang, A.; Zhang, W.; Yang, C.; Xu, T. Estimation of Maize Biomass at Multi-Growing Stage Using Stem and Leaf Separation Strategies with 3D Radiative Transfer Model and CNN Transfer Learning. *Remote Sens.* **2024**, *16*, 3000. [CrossRef]
29. Ma, J.; Yuan, C.; Zhou, J.; Li, Y.; Gao, G.; Fu, B. Logistic Model Outperforms Allometric Regression to Estimate Biomass of Xerophytic Shrubs. *Ecol. Indic.* **2021**, *132*, 108278. [CrossRef]
30. Yang, Q.; Su, Y.; Hu, T.; Jin, S.; Liu, X.; Niu, C.; Liu, Z.; Kelly, M.; Wei, J.; Guo, Q. Allometry-Based Estimation of Forest Aboveground Biomass Combining LiDAR Canopy Height Attributes and Optical Spectral Indexes. *For. Ecosyst.* **2022**, *9*, 100059. [CrossRef]
31. Liu, Y.; Fan, Y.; Yue, J.; Jin, X.; Ma, Y.; Chen, R.; Bian, M.; Yang, G.; Feng, H. A Model Suitable for Estimating Above-Ground Biomass of Potatoes at Different Regional Levels. *Comput. Electron. Agric.* **2024**, *222*, 109081. [CrossRef]
32. Liu, Y.; Feng, H.; Yue, J.; Jin, X.; Fan, Y.; Chen, R.; Bian, M.; Ma, Y.; Li, J.; Xu, B.; et al. Improving Potato AGB Estimation to Mitigate Phenological Stage Impacts through Depth Features from Hyperspectral Data. *Comput. Electron. Agric.* **2024**, *219*, 108808. [CrossRef]

33. Lancashire, P.D.; Bleiholder, H.; Boom, T.V.D.; Langelüddeke, P.; Stauss, R.; Weber, E.; Witzenberger, A. A Uniform Decimal Code for Growth Stages of Crops and Weeds. *Ann. Appl. Biol.* **1991**, *119*, 561–601. [CrossRef]
34. Zadoks, J.C.; Chang, T.T.; Konzak, C.F. A Decimal Code for the Growth Stages of Cereals. *Weed Res.* **1974**, *14*, 415–421. [CrossRef]
35. Han, S.; Zhao, Y.; Cheng, J.; Zhao, F.; Yang, H.; Feng, H.; Li, Z.; Ma, X.; Zhao, C.; Yang, G. Monitoring Key Wheat Growth Variables by Integrating Phenology and UAV Multispectral Imagery Data into Random Forest Model. *Remote Sens.* **2022**, *14*, 3723. [CrossRef]
36. Mcmaster, G. Growing Degree-Days: One Equation, Two Interpretations. *Agric. For. Meteorol.* **1997**, *87*, 291–300. [CrossRef]
37. Yue, J.; Yang, G.; Tian, Q.; Feng, H.; Xu, K.; Zhou, C. Estimate of Winter-Wheat above-Ground Biomass Based on UAV Ultrahigh-Ground-Resolution Image Textures and Vegetation Indices. *ISPRS J. Photogramm. Remote Sens.* **2019**, *150*, 226–244. [CrossRef]
38. Curtis, B.C.; Rajaram, S.; Gómez Macpherson, H.; FAO. (Eds.) *Bread Wheat: Improvement and Production*; FAO Plant Production and Protection Series; Food and Agriculture Organization of the United Nations: Rome, Italy, 2002; ISBN 978-92-5-104809-2.
39. Rouse, J.W.; Haas, R.H.; Scheel, J.A.; Deering, D.W. Monitoring Vegetation Systems in the Great Plains with ERTS. In *3rd Earth Resource Technology Satellite (ERTS) Symposium*; Scientific and Technical Information Office, National Aeronautics and Space Administration: Washington, DC, USA, 1974; Volume 1, pp. 48–62.
40. Gitelson, A.A.; Gritz, Y.; Merzlyak, M.N. Relationships between Leaf Chlorophyll Content and Spectral Reflectance and Algorithms for Non-Destructive Chlorophyll Assessment in Higher Plant Leaves. *J. Plant Physiol.* **2003**, *160*, 271–282. [CrossRef]
41. Gitelson, A.; Merzlyak, M.N. Spectral Reflectance Changes Associated with Autumn Senescence of *Aesculus hippocastanum* L. and *Acer platanoides* L. Leaves. Spectral Features and Relation to Chlorophyll Estimation. *J. Plant Physiol.* **1994**, *143*, 286–292. [CrossRef]
42. Féret, J.-B.; François, C.; Gitelson, A.; Asner, G.P.; Barry, K.M.; Panigada, C.; Richardson, A.D.; Jacquemoud, S. Optimizing Spectral Indices and Chemometric Analysis of Leaf Chemical Properties Using Radiative Transfer Modeling. *Remote Sens. Environ.* **2011**, *115*, 2742–2750. [CrossRef]
43. Serrano, L.; Penuelas, J.; Ustin, S.L. Remote Sensing of Nitrogen and Lignin in Mediterranean Vegetation from AVIRIS Data: Decomposing Biochemical from Structural Signals. *Remote Sens. Environ.* **2002**, *81*, 355–364. [CrossRef]
44. Lemaire, G.; Francois, C.; Soudani, K.; Berveiller, D.; Pontailler, J.; Breda, N.; Genet, H.; Davi, H.; Dufrene, E. Calibration and Validation of Hyperspectral Indices for the Estimation of Broadleaved Forest Leaf Chlorophyll Content, Leaf Mass per Area, Leaf Area Index and Leaf Canopy Biomass. *Remote Sens. Environ.* **2008**, *112*, 3846–3864. [CrossRef]
45. Montesinos-López, O.A.; Martín-Vallejo, J.; Crossa, J.; Gianola, D.; Hernández-Suárez, C.M.; Montesinos-López, A.; Juliana, P.; Singh, R. A Benchmarking Between Deep Learning, Support Vector Machine and Bayesian Threshold Best Linear Unbiased Prediction for Predicting Ordinal Traits in Plant Breeding. *G3 Genes | Genomes | Genet.* **2019**, *9*, 601–618. [CrossRef] [PubMed]
46. Li, Z.; Zhao, Y.; Taylor, J.; Gaulton, R.; Jin, X.; Song, X.; Li, Z.; Meng, Y.; Chen, P.; Feng, H.; et al. Comparison and Transferability of Thermal, Temporal and Phenological-Based in-Season Predictions of above-Ground Biomass in Wheat Crops from Proximal Crop Reflectance Data. *Remote Sens. Environ.* **2022**, *273*, 112967. [CrossRef]
47. Li, Z.; Taylor, J.; Yang, H.; Casa, R.; Jin, X.; Li, Z.; Song, X.; Yang, G. A Hierarchical Interannual Wheat Yield and Grain Protein Prediction Model Using Spectral Vegetative Indices and Meteorological Data. *Field Crops Res.* **2020**, *248*, 107711. [CrossRef]
48. Hu, Z.; Chen, D.; Chen, X.; Zhou, Q.; Peng, Y.; Li, J.; Sang, Y. CCHZ-DISO: A Timely New Assessment System for Data Quality or Model Performance From Da Dao Zhi Jian. *Geophys. Res. Lett.* **2022**, *49*, e2022GL100681. [CrossRef]
49. Feng, Z.; Cheng, Z.; Ren, L.; Liu, B.; Zhang, C.; Zhao, D.; Sun, H.; Feng, H.; Long, H.; Xu, B.; et al. Real-Time Monitoring of Maize Phenology with the VI-RGS Composite Index Using Time-Series UAV Remote Sensing Images and Meteorological Data. *Comput. Electron. Agric.* **2024**, *224*, 109212. [CrossRef]
50. Zeng, N.; Ren, X.; He, H.; Zhang, L.; Zhao, D.; Ge, R.; Li, P.; Niu, Z. Estimating Grassland Aboveground Biomass on the Tibetan Plateau Using a Random Forest Algorithm. *Ecol. Indic.* **2019**, *102*, 479–487. [CrossRef]
51. Huang, H.; Huang, J.; Li, X.; Zhuo, W.; Wu, Y.; Niu, Q.; Su, W.; Yuan, W. A Dataset of Winter Wheat Aboveground Biomass in China during 2007–2015 Based on Data Assimilation. *Sci Data* **2022**, *9*, 200. [CrossRef]
52. Li, P.; Zhang, X.; Wang, W.; Zheng, H.; Yao, X.; Tian, Y.; Zhu, Y.; Cao, W.; Chen, Q.; Cheng, T. Estimating Aboveground and Organ Biomass of Plant Canopies across the Entire Season of Rice Growth with Terrestrial Laser Scanning. *Int. J. Appl. Earth Obs. Geoinf.* **2020**, *91*, 102132. [CrossRef]
53. Jungers, J.M.; Frahm, C.S.; Tautges, N.E.; Ehlke, N.J.; Wells, M.S.; Wyse, D.L.; Sheaffer, C.C. Growth, Development, and Biomass Partitioning of the Perennial Grain Crop *Thinopyrum Intermedium*: Growth, Development, and Biomass Partitioning of a Perennial Grain Crop. *Ann. Appl. Biol.* **2018**, *172*, 346–354. [CrossRef]
54. Zhang, J.; Zhao, Y.; Hu, Z.; Xiao, W. Unmanned Aerial System-Based Wheat Biomass Estimation Using Multispectral, Structural and Meteorological Data. *Agriculture* **2023**, *13*, 1621. [CrossRef]
55. Qiao, K. New Three Red-Edge Vegetation Index (VI3RE) for Crop Seasonal LAI Prediction Using Sentinel-2 Data. *Int. J. Appl. Earth Obs. Geoinf.* **2024**, *130*, 103894. [CrossRef]
56. Sun, Y.; Wang, B.; Zhang, Z. Improving Leaf Area Index Estimation With Chlorophyll Insensitive Multispectral Red-Edge Vegetation Indices. *IEEE J. Sel. Top. Appl. Earth Obs. Remote Sens.* **2023**, *16*, 3568–3582. [CrossRef]
57. Dong, Q.; Chen, X.; Chen, J.; Zhang, C.; Liu, L.; Cao, X.; Zang, Y.; Zhu, X.; Cui, X. Mapping Winter Wheat in North China Using Sentinel 2A/B Data: A Method Based on Phenology-Time Weighted Dynamic Time Warping. *Remote Sens.* **2020**, *12*, 1274. [CrossRef]

58. Li, C.; Chen, W.; Wang, Y.; Wang, Y.; Ma, C.; Li, Y.; Li, J.; Zhai, W. Mapping Winter Wheat with Optical and SAR Images Based on Google Earth Engine in Henan Province, China. *Remote Sens.* **2022**, *14*, 284. [CrossRef]
59. He, J.; Zhang, N.; Su, X.; Lu, J.; Yao, X.; Cheng, T.; Zhu, Y.; Cao, W.; Tian, Y. Estimating Leaf Area Index with a New Vegetation Index Considering the Influence of Rice Panicles. *Remote Sens.* **2019**, *11*, 1809. [CrossRef]
60. Li, D.; Yu, W.; Zheng, H.; Guo, C.; Yao, X.; Zhu, Y.; Cao, W.; Cheng, T. Towards Practical Semi-Empirical Models for the Estimation of Leaf and Canopy Water Contents from Hyperspectral Reflectance. *Comput. Electron. Agric.* **2023**, *214*, 108309. [CrossRef]
61. Mutanga, O.; Masenyama, A.; Sibanda, M. Spectral Saturation in the Remote Sensing of High-Density Vegetation Traits: A Systematic Review of Progress, Challenges, and Prospects. *ISPRS J. Photogramm. Remote Sens.* **2023**, *198*, 297–309. [CrossRef]
62. Li, L.; Mu, X.; Jiang, H.; Chianucci, F.; Hu, R.; Song, W.; Qi, J.; Liu, S.; Zhou, J.; Chen, L.; et al. Review of Ground and Aerial Methods for Vegetation Cover Fraction (fCover) and Related Quantities Estimation: Definitions, Advances, Challenges, and Future Perspectives. *ISPRS J. Photogramm. Remote Sens.* **2023**, *199*, 133–156. [CrossRef]
63. Zhu, C.; Liu, S.; Parent, B.; Yin, X.; De Solan, B.; Jiang, D.; Ding, Y.; Baret, F. Genotype × Environment × Management Analysis to Define Allometric Rules between Leaves and Stems in Wheat. *J. Exp. Bot.* **2024**, *75*, 6388–6404. [CrossRef]